High-Throughput Synthesis, Screening and Scale-Up of Optimised Conducting Indium Tin Oxides.

Peter Marchand,[a] Neel M. Makwana,[a] Christopher J. Tighe,[b] Robert I. Gruar,[a] Ivan P. Parkin,[a] Claire J. Carmalt[a] and Jawwad A. Darr*[a]

[a] Christopher Ingold Laboratories, Department of Chemistry, University College London, 20 Gordon Street, London, WC1H 0AJ, UK. E-mail: j.a.darr@ucl.ac.uk

[b] Department of Chemical Engineering, Imperial College London, South Kensington Campus, London, SW7 2AZ, UK.

Abstract

A high-throughput optimisation and subsequent scale-up methodology has been used for the synthesis of conductive tin-doped indium oxide (known as ITO) nanoparticles. ITO nanoparticles with up to 12 at% Sn were synthesised using a laboratory scale (15 g/hour by dry mass) continuous hydrothermal synthesis process and the as-synthesised powders were characterised by powder X-ray diffraction (XRD), transmission electron microscopy (TEM), energy-dispersive X-ray analysis (EDXA) and X-ray photoelectron spectroscopy (XPS). Under standard synthetic conditions, either the cubic In_2O_3 phase, or a mixture of InO(OH) and In_2O_3 phases were observed in the as-synthesised materials. These materials were pressed into compacts, heat-treated in an inert atmosphere and their electrical resistivities were then measured using the Van der Pauw method. Sn-doping yielded resistivities of ~ 10^{-2} Ω cm for most samples, with the lowest resistivity of 6.0 x 10^{-3} Ω cm (exceptionally conductive for such pressed nanopowders) at a Sn concentration of 10 at%. Thereafter, the optimised lab-scale composition was scaled-up using a pilot scale continuous hydrothermal synthesis process (at a rate of 100 g/hour by dry mass) and a comparable resistivity of 9.4 x 10^{-3} Ω cm was obtained. The use of the synthesised TCO nanomaterials for thin film fabrication was finally demonstrated by deposition of a transparent, conductive film using a simple spin-coating process.

Introduction

The combination of low electrical resistivity and high optical transparency, make transparent conducting oxides (TCOs) one of the most important classes of advanced functional materials.[1,2] These unique properties are vital in the development of applications such as solar cells,[2,3] smart windows,[4] organic light emitting diodes (OLEDs),[5] touch screens[6] and flat panel displays.[7] The simultaneous existence of high transparency and high conductivity requires the introduction of nonstoichiometry with respect to oxygen and/or suitable dopants into wide band gap (> 3 eV) oxide structures.[8] Tin-doped indium oxide (also known as

indium tin oxide, ITO) remains the industry standard TCO, with low resistivity (typically ~10^{-4} Ω cm for thin films) and high optical transparency >80 % for thin films.[1,9] Given the interest in ITO as a TCO, it is unsurprising that significant research over the last two decades has focused on the development of this material as printed ink tracks and thin films. Dense thin films of ITO can be deposited using a wide range of techniques including sputtering,[10] chemical vapour deposition[11] and pulsed laser deposition.[12] Some of these processes typically require annealing steps in excess of 700 °C in order to obtain the best performance.[8] This can restrict applications to substrates that can withstand such harsh conditions, prohibiting the use of materials such as plastic for flexible devices. The use of highly crystalline TCO nanomaterials offers potential strategies for the deposition of thin films over large scales, using well defined coating materials. Furthermore, formulation of TCO nanoparticles into dispersions, pastes and ceramic inks allows them to be deposited onto substrates *via* screen printing and inkjet processes.[13–15] When such approaches are coupled with fast, low-temperature or rapid heat-processing, they offer inexpensive and potentially more environmentally friendly approaches for the large-scale manufacture of printed optoelectronics.[16]

In order to achieve high performance TCO printed tracks or coatings from particles, control over size, morphology and particularly structural defects (such as oxygen vacancies) is determined by the synthetic conditions used. The formation of ITO nanomaterials has included techniques such as batch coprecipitation and batch solvothermal/hydrothermal methods.[13,17–20] In particular, microwave-assisted solvothermal syntheses have yielded powders with particularly low resistivities when pressed into a pellet (*ca.* 1.2 x 10^{-2} Ω cm).[1321,22] However, the relevance of such synthetic approaches to industrial scale-up is limited because of the use of toxic organic solvents with high Volatile Organic Compound (VOC) content, as well as batch to batch variations in the static processes.

Continuous hydrothermal flow synthesis (CHFS) processes offer the potential for controlled and consistent syntheses of nanomaterials at scale. In such processes, metal oxide nanoparticles are typically formed upon mixing a feed of supercritical (or superheated) water with a stream of aqueous metal salts at ambient-temperature.[23] This environment rapidly converts the precursors into nanoparticulate metal oxides by simultaneous hydrolysis and dehydration of the metal salt to the oxide. In continuous hydrothermal reactors, the mixing approach by which supercritical water is mixed with metal precursor solutions can affect the properties of the nanoparticles formed.[24] Recently, the use of a Confined Jet Mixer (CJM) has

been reported for the continuous synthesis of nanoparticles, in which a flow of aqueous precursors is entrained in a jet of supercritical water, affording rapid mixing, generally under turbulent conditions.[25–27]

For the discovery and optimisation of TCO nanomaterials, the development of high-throughput synthesis and screening methods for doped metal oxide systems, is highly desirable. Such doped metal oxide systems can be easily made by incorporation of additional metal salts into the CHFS process. One particular benefit of such modified CHFS reactors, is that many different compositions of doped materials can be synthesised in a short time and sequentially by simply adjusting the relative concentrations of the metal precursors used (and taking care to avoid cross-contamination).[28] Variations of this high-throughput approach for CHFS has been previously demonstrated by some of the authors previously, e.g. in the synthesis of an entire $Ce_xZr_yY_zO_{2-\delta}$ phase diagram,[29] Eu-doped $Y(OH)_3$ libraries,[30] Fe-doped $La_4Ni_3O_{10}$ libraries[31] and rare earth element doped zinc oxide libraries.[28] Application of this high throughput approach to TCO materials discovery, would be expected to facilitate rapid optimisation of high conductivity TCOs by variation in dopant or reagent levels.

The use of CHFS for the direct synthesis of In_2O_3 nanoparticles used in a gas sensing application has been previously demonstrated by some of the authors using both small-scale and pilot scale continuous hydrothermal flow reactors.[32,33] Therein, the In_2O_3 was formed directly in process as cubic (bixbyite) phase without the need of any auxiliary reagents such as [KOH]. The synthesis of ITO by a continuous hydrothermal process has been reported by Fang[34] and Lu.[35] In both those reports, InO(OH) was observed under certain conditions and reaction temperatures > 400 °C were necessary to achieve phase-pure ITO directly in-process.

In order to obtain sufficient conductivity in ITO nanomaterials, the extent of oxygen vacancies within the structure is important.[8,36,37] Oxygen vacancies act as doubly ionised donors, contributing a maximum of two electrons to the conduction band. These oxygen vacancies also allow for O^{2-} ion mobility, however, conduction arising by this pathway is negligible compared to the electronic contribution.[38] Commonly, such defects are introduced by using post-synthesis annealing under reducing atmospheres.[18] To achieve sufficiently reducing conditions within the continuous hydrothermal process (to form oxygen vacancies), one approach is to use an in situ reducing agent such as formic acid, which decomposes to CO_2 and reducing H_2 gas under supercritical conditions.[39,40]

This approach was successfully employed by Lu *et al.* for the continuous production of ITO nanoparticles with a hexanoic acid surface coating.[35] The as-synthesised material in that report was pressed (at 9.6 MPa) into compacts (density *ca.* 3.6 g cm^{-3}) which had a measured resistivity of ca. 8.3 Ω cm (reported as a conductivity of 0.12 S cm^{-1}). However, no optimisation of dopant concentration was made in the report. The observed resistivity in that case compared it to a resistivity value of 5 x 10^{-2} Ω cm reported by Sasaki *et al.* for an ITO powder made by a batch solvothermal method (note however, the pressed compacts in this latter case were also heat-treated at 300 °C under a 1% H_2 in N_2 atmosphere).[18]

Herein, we report the use of a high-throughput CHFS approach for the optimisation of conductive ITO nanomaterials, utilising formic acid as an *in situ* reducing agent for the formation of conductive materials. Nanomaterial composition optimisation was first carried out on a 'lab-scale' reactor at a production rate of 15 g/hour per sample (by dry mass) and the effects of dopant level and [KOH] auxiliary reagent on the crystallographic phase of the as-synthesised materials were studied. The lab-scale materials were screened in parallel as heat-treated pellets and the optimised composition was subsequently synthesised using a pilot-scale CHFS reactor at a production rate of 100 g/hour (by dry mass) and the conductivity of this material was also evaluated as a heat-treated pellet. The work carried out herein, represents a first demonstration of the use of high-throughput CHFS synthesis and scale-up of an optimised TCO nanomaterial and can be broadly applied to a number of inorganic materials discovery areas, as long as suitable screening methods are available.

Experimental

Materials

Reagents were purchased from the following suppliers and used as-purchased: indium(III) nitrate hydrate, 99 % (Alfa Aesar, Lancashire, UK); potassium stannate trihydrate, 99.9 % (Sigma Aldrich, Dorset, UK); potassium hydroxide (Fisher Scientific, Leicestershire, UK); formic acid, ≥95 % (Sigma Aldrich, Dorset, UK).

Nanoparticle Synthesis by CHFS. Table 1 contains experimental details of the conditions used in the synthesis of samples 1 - 12. The following is a description of representative procedures, with full experimental details for all samples given in the Supporting Information. Figure 1 shows a simplified flow diagram of the CHFS process used for the synthesis of the nanoparticles. In general, three diaphragm pumps (Primeroyal K, Milton

Roy, Pont-Saint-Pierre, France) were used to supply feeds of deionised water (P_{sw}), an aqueous solution of indium(III) nitrate hydrate (P_{In}) and an aqueous solution of potassium stannate trihydrate (P_{Sn}). Where KOH was incorporated, it was mixed with the Sn precursor solution supplied by P_{Sn}. Where formic acid was used, it was supplied by a fourth diaphragm pump, designated P_{FA}.

The DI water feed from pump P_{SW} was heated in flow to 450 °C using a 7 kW custom-built in-line electrical heater and was mixed with the flow of (room temperature) aqueous formic acid from pump P_{FA} at mixing point M1, shown in Figure 1. Precursor feeds from pumps P_{In} and P_{Sn}, were separately mixed in a T-piece (at room temperature) prior to mixing with the combined superheated water/formic acid feed in the confined jet mixer (CJM), which is shown as M2 in Figure 1. The design of the CJM is detailed in previous publications of the authors.[24–26] In the case of samples 5 and 11, P_{FA} was omitted and the feed of supercritical water was mixed directly with the combined precursor feed at M2. In all cases, the total concentration of the metal precursors in the initial precursor feed was maintained at 0.1 M, with the atomic ratio of the indium and tin precursors being varied according to desired tin-loading of the product. Thus, for a desired In:Sn atomic ratio of 90:10, precursor solution concentrations of 0.09 and 0.01 M were used In and Sn, respectively.

The particle-laden flow in the CHFS process was then cooled to ~40°C using a 1.5 m pipe-in pipe counter-current heat exchanger, before the slurry passed through a back-pressure regulator (BPR) valve. The aqueous nanoparticle slurry exiting the BPR was collected in a beaker and then cleaned by repeated centrifugation and washing with deionised water, until the conductivity of the supernatant was consistently below 50 μS, as measured by a conductivity probe (Hanna Instruments, model HI98311). The concentrated slurry was then freeze-dried (Virtis Genesis 35XL) by slowly heating a sample from -60 to 25 °C (over 24 h) under vacuo (< 100 mTorr), which yielded free-flowing nanoparticulate powders.

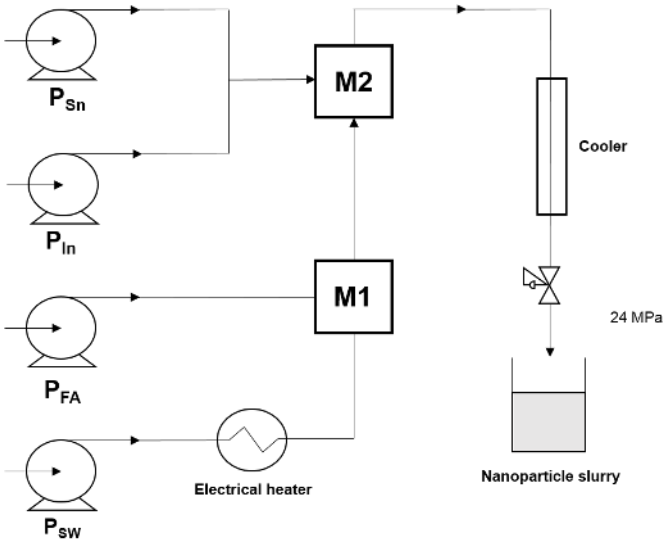

Figure 1 - Schematic diagram representing the CHFS process. Detailed diagrams of the mixer arrangements used in this study are given in the Supporting Information.

Table 1 - A description of experimental conditions used in the synthesis of ITO nanoparticles by CHFS.

Sample no.	**In:Sn atomic ratio[a]**	**[KOH] / M**	**[HCOOH] / M**	**Temp. at reaction point M2 / °C[b]**	**As-synthesised XRD Phase**	**Product Yield (%)**
Lab-scale synthesis/optimisation						
1	90:10	0.1	1	350	InO(OH)	57
2	90:10	0.2	1	350	In_2O_3 / InO(OH)	63
3	90:10	0.3	1	350	In_2O_3* / InO(OH)[†]	70
4	90:10	0.3	0	350	In_2O_3* / InO(OH) [†]	66
Synthesis of In_2O_3						
5	100:0	0	0	305	In_2O_3	64
6	90:10	0	0	305	InO(OH)	75
ITO dopant screening						
7	100:0	0.3	1	350	In_2O_3* / InO(OH)[†]	47
8	96:4	0.3	1	350	In_2O_3* / InO(OH)[†]	64
9	94:6	0.3	1	350	In_2O_3* / InO(OH)[†]	56
10	92:8	0.3	1	350	In_2O_3* / InO(OH)[†]	68
11	88:12	0.3	1	350	In_2O_3* / InO(OH)[†]	74
Pilot-plant synthesis						
12	90:10	0.75	0.5	350	In_2O_3 / InO(OH)	71

Key: a) The total concentration of metal ions (In + Sn) for samples 1-11 was 0.1 M; b) Temperatures calculated based on the properties of the fluids and the temperatures and flow rates used;[41]
* Indicates major phase observed; † Indicates minor phase observed.

Materials Characterisation

Powder X-ray diffraction (XRD) data were collected using a STOE Stadi P diffractometer (Mo-Ka radiation, 0.70932 Å) in transmission geometry. Data were collected over the 2θ range 5 - 30° with a step size of 0.5° and a count time of 20 s per step. Transmission electron microscopy (TEM) was performed using a Jeol 200 kV transmission electron microscope in imaging mode. Cleaned samples were dispersed in MeOH and drop coated onto a carbon coated copper TEM grid purchased from Agar Scientific. Image analysis and particle size measurements were carried out on 300 particles for each sample using ImageJ software. Energy Dispersive X-ray (EDX) analysis was carried out using an Oxford Instruments X-Max^N 80-T Silicon Drift Detector (SDD) fitted to the transmission electron microscope and process using AZtec® software. X-ray photoelectron spectroscopy (XPS) was performed a Thermo Scientific K-alpha photoelectron spectrometer using monochromatic Al-Kα radiation. Survey scans were collected in the range 0 – 1100 eV (binding energy) at a pass energy of 160 eV. Higher resolution scans were recorded for the principal peaks of In (3d), Sn (3d), O (1s) and C (1s) at a pass energy of 50 eV. Peak positions were calibrated to carbon and plotted using the CasaXPS software.

To assess the conductivity of the materials, the powders were pressed into compacts of thickness 1.6 mm under a force of 50 kN using a hydraulic press (Specac, Orpington, UK). The deep blue coloured discs were then heat-treated under argon at 600 °C for 3 hours and after cooling to room temperature, the disks were green in colour. Hall effect measurements were carried out using the Van der Pauw method to determine the bulk resistivity of the disks. In order to do this, gold contacts were first sputtered onto the heat-treated discs, which were then subjected to an input current of 1 mA and a calibrated magnetic field of 0.58 T. The transverse voltage was then measured. The measurement was repeated by reversing the direction of the magnetic field and the current. Resistivity measurements were made three times for each pellet in each direction and the mean value and standard deviations calculated. A thin film was deposited by spin coating from a 20 wt% dispersion of sample 12 in water using a Laurell WS-650-23B spin coater.

Results & Discussion

Synthesis and characterisation of ITO nanopowders

Initial doping investigations maintained a constant tin loading of 10 at% (with respect to In) by addition of [$K_2SnO_3 \cdot 3H_2O$] at the appropriate concentration through a secondary feed supplied by pump P_{Sn}. The influence of adding formic acid on the reaction was investigated by pre-mixing of a 1 M aqueous feed of formic acid with the supercritical water feed in the process. Under the supercritical conditions within the reactor, formic acid is known to decompose to CO_2 and H_2,[40] which would be expected to create the reducing conditions required to promote the formation of oxygen vacancies within the ITO structure.[35] In the absence of formic acid, an off-white material was produced. In contrast, the inclusion of formic acid in the process led to a light blue product being formed. This colouration of ITO suggested the formation of some oxygen vacancies within the structure (and presumably an increase in carrier concentration).[35,42]

The influence of base as an auxiliary reagent was also investigated by the addition of KOH (in the range 0.1 – 0.3 M) with the tin precursor feed issuing from pump P_{Sn}. Initial investigations used a Sn feed concentration of 10 at% with respect to the indium precursor feed concentration. Powder X-ray diffraction analysis of the as-produced materials revealed a

mixture of InO(OH) and In_2O_3 (bixbyite) phases

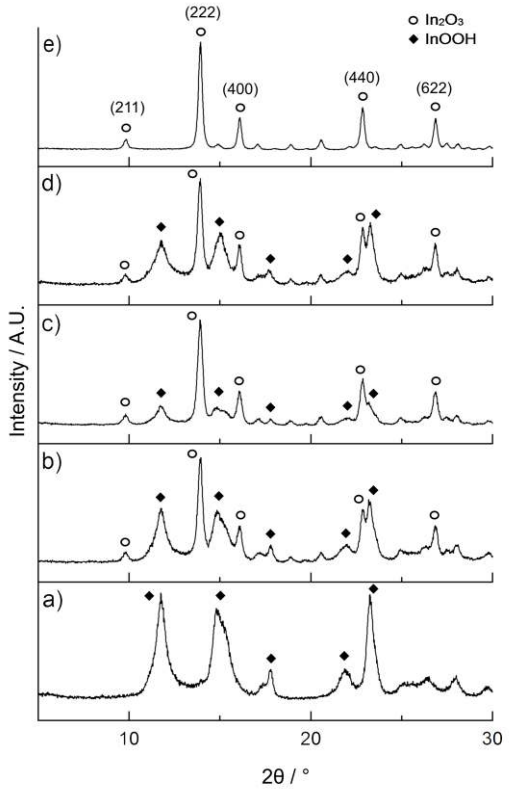

(

*Figure 2*a-c). At the lowest concentration of KOH, only the InO(OH) phase was observed. Increasing [KOH] to 0.3 M, resulted in the formation of predominantly the bixbyite oxide phase, although a minor InO(OH) phase was still observed. Further increase in [KOH] to 0.6 M yielded no significant difference in the phase-purity of the product, with a mixture of phases still being present (Figure 2d).

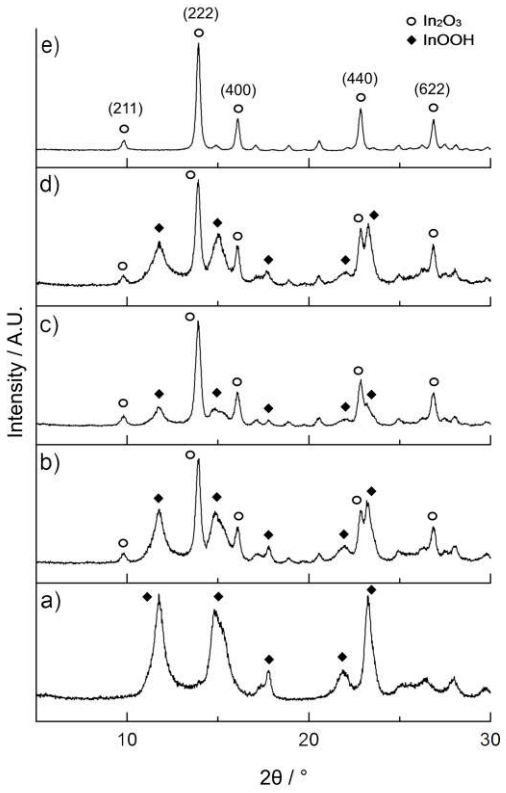

Figure 2 –Powder XRD patterns of ITO nanomaterials synthesised by CHFS with 10 at% Sn. a) sample 1, as prepared; b) sample 2, as prepared; c) sample 3, as prepared; d) sample 4, as prepared; e) sample 3, heat-treated.

To further examine the phase behaviour of the system, syntheses were carried out in the absence of KOH and formic acid, mimicking the conditions used for the previous synthesis of phase-pure undoped In_2O_3 by a smaller scale CHFS process (3.75 times smaller than the lab-scale reactor used herein, based on total volumetric flow rates).[32] It was found that in the absence of the Sn dopant (sample 5) phase-pure In_2O_3 was formed, whereas only InO(OH) was observed when the Sn dopant was included (sample 6), as shown in Figure S4 (Supporting Information). Thus, the observed phase impurity was attributed to additional presence of the Sn precursor, which appeared to retard the exclusive formation of the bixbyite phase compared to the undoped indium oxide.

The phase purity of hydrothermally-made ITO nanomaterials by continuous methods was previously reported to have a high dependence on the reaction temperature due to the very short reaction times involved in comparison to batch methods.[34,35] Lu *et al.* reported the continuous synthesis of ITO requiring reaction temperatures quoted at >400 °C for the

formation of phase-pure bixbyite ITO.[35] In the absence of base, the hydrothermal synthesis of In_2O_3 is understood to proceed by the initial hydrolysis of In^{3+} to form $In(OH)_3$, followed by partial dehydration to InO(OH) and subsequent complete dehydration to In_2O_3 (see equations 1 – 3 below):[20]

$$In^{3+} + 3\,H_2O \rightarrow In(OH)_3 + 3\,H^+ \qquad (1)$$

$$In(OH)_3 \rightarrow InOOH + H_2O \qquad (2)$$

$$2\,InOOH \rightarrow In_2O_3 + H_2O \qquad (3)$$

With the addition of KOH, $In(OH)_3$ was formed in flow upon mixing of the aqueous precursor feeds under ambient conditions, allowing for an overall increase in the rate of formation of In_2O_3 (by the subsequent two-step dehydration) upon mixing with the supercritical water feed.

Heat-treatment of all the as-prepared materials under an argon atmosphere at 600 °C for 3

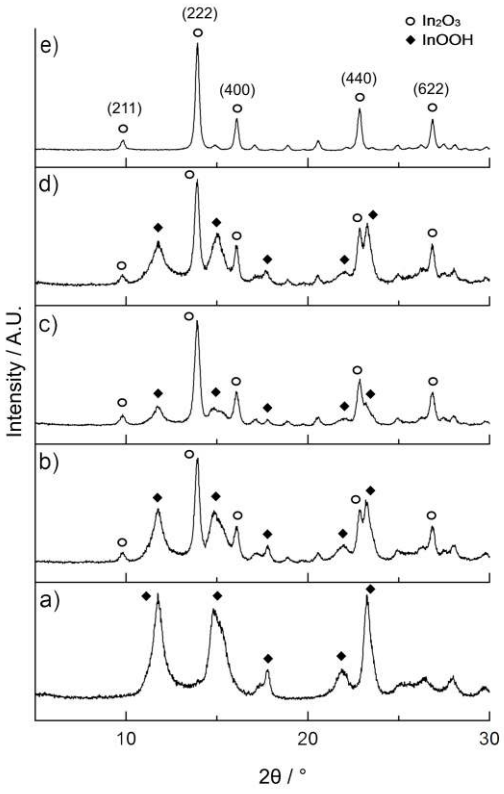

hours in a tube furnace (

*Figure 2*e), yielded phase-pure cubic (bixbyite) ITO. In the powder XRD data, a characteristic intense (222) peak was observed at $2\theta = 13.9°$, while other strong but less intense peaks were observed at $2\theta = 16.1$, 22.8 and 26.9 °, which were attributed to the (400), (440) and (662) planes, respectively. The broad nature of the XRD peaks for both the as-prepared and heat-treated materials was indicative of the nano-sized particles.

Amongst the as-synthesised Sn-doped In_2O_3/InO(OH) mixed phase samples, sample 3 had the highest phase purity, thus this sample was investigated further using transmission electron microscopy (TEM), as shown in Figure 3. The images revealed well-defined cube-like particles with rounded edges (Figure 3b). High resolution TEM (HRTEM) imaging (Figure 3c) revealed the highly crystalline nature of the nanoparticles. A lattice spacing of 0.25 nm was identified, which corresponded to the interplanar spacing of the (400) planes of cubic ITO. The selected area diffraction pattern (as shown in the inset of Figure 3c), was indexed to confirm the formation of the cubic ITO, when referenced to the powder XRD pattern. In this way, some of the as-prepared particles could also be indexed to confirm the presence of the orthorhombic InO(OH) phase, in agreement with the observations made by powder XRD. No phases corresponding to SnO_2 or $In(OH)_3$ were observed in either powder XRD or HRTEM / SAED analyses. From TEM micrographs, all particles measured for sample 3 were found to be within the range 7 – 31 nm, with a mean particle size of 15.1 ± 4.1 nm.

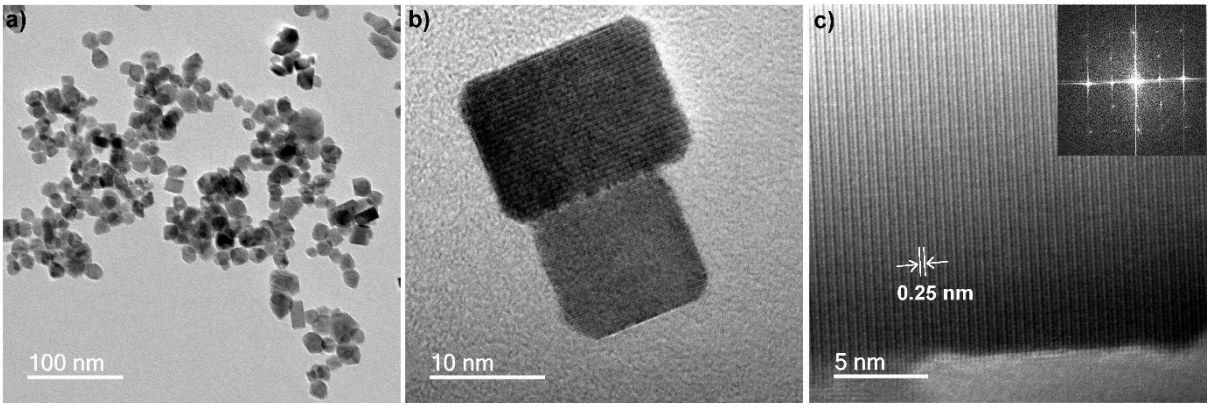

Figure 3 - TEM images of ITO nanoparticles (sample 3) synthesised by CHFS. a) 25,000 x magnification; b) 300,000 x magnification; c) 500,000 x magnification. Inset: selected area electron diffraction (SAED) pattern.

The elemental composition of the nanoparticles was investigated by STEM/EDX and XPS analysis. STEM/EDX showed a homogenous distribution of the Sn dopant within the material and no separation of any tin oxide phases (Figure S5). The compositional analysis of sample 3 suggested a Sn loading of 9.5 at%, which was close to the input tin precursor concentration

of 10 at% (with respect to indium) used in the CHFS process. XPS analysis confirmed the presence of indium and tin within the sample by the presence of peaks at 444.5 and 486.6 eV, corresponding to the $3d_{5/2}$ levels of In^{3+} and Sn^{4+}, respectively.[43,44] In both cases, the high resolution spectra could be fitted with a single set of doublet peaks, indicating the presence of only one chemical species for each element (Figure S6).

High-throughput Screening of ITO Nanomaterials

The synthetic strategy implemented in this work for the optimisation and scale-up production of ITO nanoparticles is outlined in Figure 4.

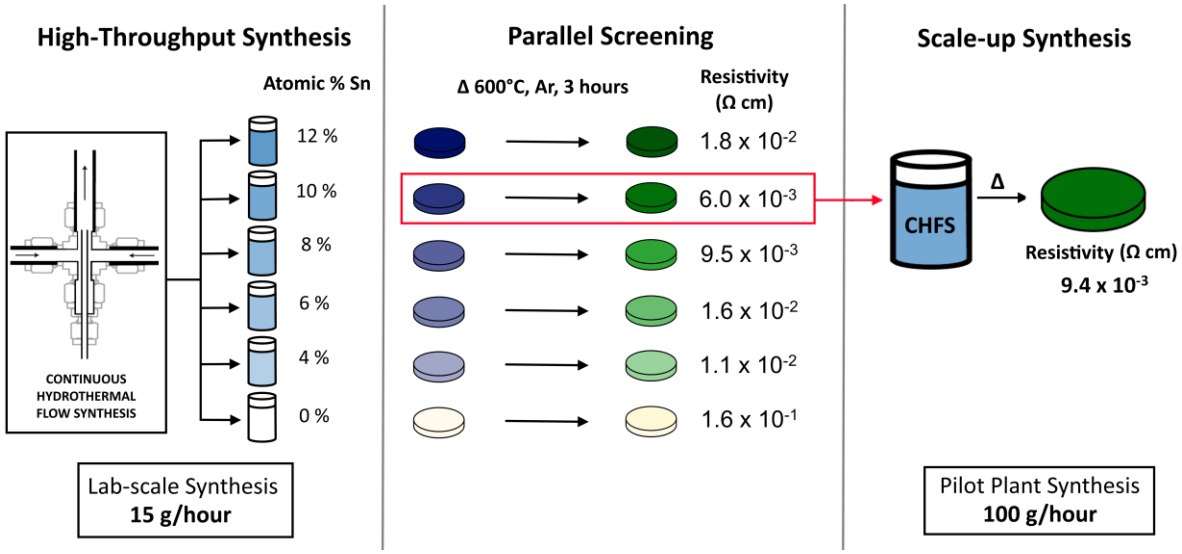

Figure 4 - Representation of TCO nanomaterial lab scale synthesis (lab scale CHFS), parallel screening and scale-up strategy (pilot scale SHFS).

In order to determine the optimum dopant concentration, ITO nanopowders with varying Sn concentrations were sequentially synthesised by setting the initial concentrations of Sn in the range 0 to 12 at% with respect to In. Approximately 0.75 g of each of the as-synthesised powders was pressed into a 1.6 mm thick and 16 mm diameter cylindrical pellet (density = *ca.* 2.3 g cm^{-3}) to minimise grain boundary influences and enhance inter-particle contact. Heat-treatment of the pellets at 600 °C under argon for 3 hours in a tube furnace afforded phase-pure ITO (as determined by powder XRD), which resulted in a change in colour from blue to green.

The resistivity of the materials as a function of tin content is shown in Figure 5 and full Hall probe data and standard deviations are given in the Supporting Information, table S1.

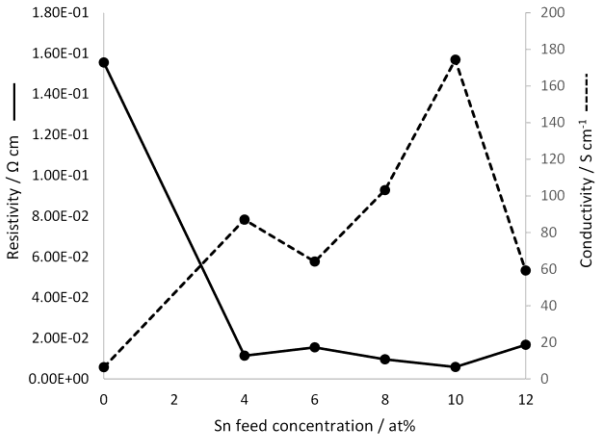

Figure 5 - Variation of bulk resistivity and conductivity with tin precursor concentration for ITO powder synthesised by CHFS. Standard deviations are omitted for clarity, full S.D. data are given in Supporting Information table S1.

Whilst undoped In_2O_3 had a bulk resistivity of 1.6 x 10^{-1} (± 3.1 x 10^{-4}) Ω cm, Sn-doping led to an immediate decrease in resistivity for all loadings, ranging from 1.2 x 10^{-2} (± 5.0 x 10^{-4}) Ω cm for 4 at% Sn, to 6.0 x 10^{-3} (± 2.1 x 10^{-4}) Ω cm for 10 at% Sn, as expected for the substitution of In^{3+} for Sn^{4+}. Materials synthesised in the absence of formic acid showed poor conductivity, owing to charge compensation by the formation of oxygen interstitials under these conditions. The reductive conditions induced by the addition of formic acid in process inhibited this charge compensation mechanism, as well as promoting the formation of oxygen vacancies within the structure, providing a further conduction mechanism.

A general decrease in resistivity was observed with increasing tin loadings in the range 4 to 10 at%, after which an increase in tin concentration resulted in an increase in resistivity. Optimum Sn concentrations in the range 5 to 10 at% have previously been observed for ITO nanopowders, with an increased resistivity at concentrations above 10 at% being attributed to phase separation of SnO_2 at higher loadings.[18] However, no evidence of SnO_2 phase separation was observed in either powder XRD or XPS analyses herein. Tomonaga *et al.* attributed this increase in resistivity with increasing Sn content to the presence of Sn interstitials, which act as scattering centres, causing a decrease in Hall mobility.[45] The lowest measured resistivity reported herein of 6.0 x 10^{-3} (± 2.1 x 10^{-4}) Ω cm was found for the sample with 10 at% Sn (sample 3), which corresponded to a conductivity of 174 (± 12.3) S cm^{-1}. Whilst this resistivity remains an order of magnitude larger than values observed for ITO thin films (*ca.* 10^{-4} Ω cm),[46] the result is still a significant improvement on the lowest reported resistivity of 1.2 x 10^{-2} Ω cm for pressed nanopowder pellets achieved by

Hammarberg *et al.* (using powders synthesised by a microwave-assisted solvothermal process).[22] In contrast to the work of Hammarberg *et al.*, herein, a post-synthesis annealing step was necessary to achieve phase-purity and minimise resistivity. The observed resistivity herein was lower than reported for ITO synthesised *via* a batch solvothermal method followed by reductive annealing in 1% H_2 in N_2 (5 x 10^{-2} Ω cm), as reported by Sasaki *et al.*.[18] This demonstrated the effectiveness of using formic acid in process for the reduction of TCO materials. Previously, the synthesis of ITO nanopowders by a continuous flow process was reported by Lu *et al.*,[35] showing a minimum resistivity of 8.3 Ω cm (reported as a conductivity of 0.1 S cm^{-1}). The resistivity reported in this work, therefore, represents a significant increase in conductivity by comparison to related TCO nanomaterial literature.

Pilot Scale Continuous Hydrothermal Synthesis of ITO

Whilst the scale of the synthesis discussed thus far (15 g/hour) was suitable for the high-throughput synthesis and screening of ITO nanomaterials, production of such materials at still larger scales is critical for practical industrial applications. Previous reports by the authors have demonstrated the scalability of the CHFS process through the synthesis of ZnO[25] and Ce-Zn oxide nanoparticles[27] in a continuous supercritical water 'pilot plant', which showed little variation from particles synthesised on the smaller 'lab-scale' process.

Owing to the superior conductivity of sample 3 on the lab-scale synthesis, a Sn dopant concentration of 10 at% was chosen for the pilot scale CHFS study. Powder XRD analysis of the synthesised particles (sample 12) revealed the formation of a mixture of InO(OH) and In_2O_3 phases in the as-prepared material, with conversion to the oxide being achieved by heat treatment at 600 °C under Argon gas for 3 hours (Figure 6a). TEM analysis revealed the formation of a mixture of spherical and rounded cube-like particle morphologies, with a mean particle size of 10.9 ± 4.6 nm. Particles were virtually indistinguishable to those formed on the lab-scale, apart from the slightly smaller average particle size (Figure 6b).

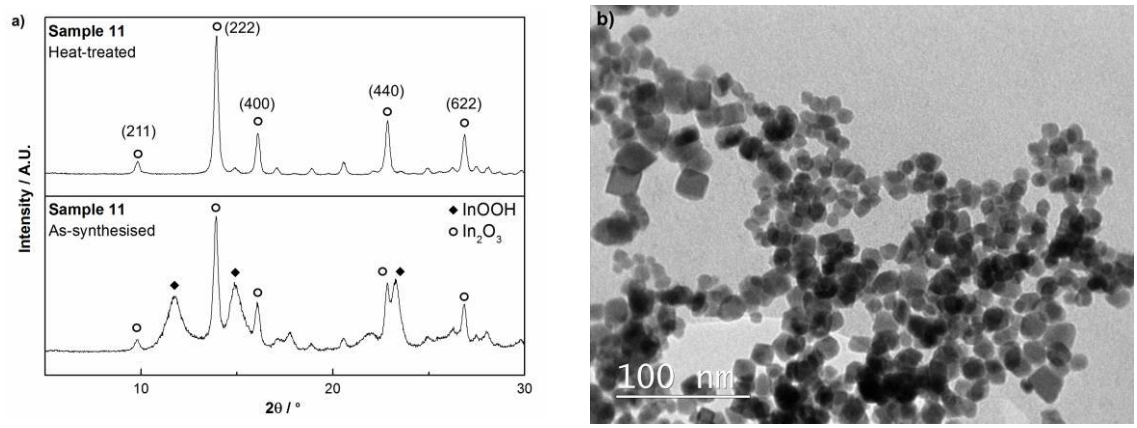

Figure 6 - a) XRD pattern of ITO nanoparticles (sample 11) synthesised on pilot-scale continuous hydrothermal reactor. Bottom: as synthesised; top: heat-treated. b) TEM image of ITO nanoparticles (sample 11).

To confirm the electrical performance of the pilot scale sample 12, compact pellets were again pressed, heat-treated and resistivity measurements were made. The resistivity of sample 12 was found to be 9.4 x 10^{-3} (± 4.8 x 10^{-4}) Ω cm, showing similar performance to the analogous material made on the 'lab scale' CHFS reactor. TEM analysis of the heat-treated sample showed retention of the small primary particle size post-treatment, with an average particle size of 13.5 ± 4.3 nm (Figure S7).

The performance of the ITO nanomaterial as a thin film was evaluated by deposition using a simple spin coating technique. A 20 wt% dispersion of sample 12 in water was deposited on a glass substrate and the resulting film was heat-treated under analogous conditions to those used for the pellets (Ar, 600 °C, 3 hours). The film showed high transparency in the visible region, with an average transmission of 84% over the wavelength range 400 – 700 nm (Supporting Information Figure S8). Furthermore, the measured resistivity of the film was 5.6 x 10^{-1} (± 1.3 x 10^{-3}) Ω cm^{-1}, based on a thickness of 23 μm measured by side-on SEM (supplementary information Figure S9), demonstrating the potential for the use of CHFS-derived TCO nanomaterials for the deposition of transparent and conductive films. Optimisation of the deposition process will lead to an improved performance of the materials as thin films. Furthermore, the use of alternative sintering processes, such as microwave sintering, will allow for the deposition of such materials onto temperature-sensitive substrates.[47] These two areas are under current investigation and will be the subject of future publications.

Conclusions

In summary, highly conductive ITO nanomaterials have been synthesised *via* continuous hydrothermal flow synthesis followed by heat-treatment of the products in an inert

atmosphere. Control over the synthetic conditions allowed the maximisation of the phase-purity in the as-prepared materials and the incorporation of formic acid provided sufficiently reducing conditions for the formation of conductive ITO.

The optimum dopant concentration was determined using a high-throughput approach, whereby dopant loadings of 0 – 12 at% Sn (with respect to In at%) within the In_2O_3 structure were rapidly synthesised in sequence. Hall effect measurements carried out on pressed pellets of the heat-treated nanopowders revealed an optimum dopant concentration of 10 at% Sn, with a resistivity of 6.0×10^{-3} ($\pm$ 2.1×10^{-4}) Ω cm. The observed conductivities measured from pressed/fired pellets gave resistivity values which were superior to the best ITO pressed powders reported in the literature to date. To our knowledge, the scale of the high throughput synthesis processes (15 g / hr) represents a relatively large scale of production for ITO nanoparticles compared to the literature. Furthermore, the use of the pilot-scale continuous hydrothermal process for the optimised ITO nanomaterial was then demonstrated at 100 g/hr (by dry mass), showing particles of very similar size and morphology to those synthesised on the lab-scale. The resistivity of the heat-treated pellets made from the pilot plant powders was 9.4×10^{-3} Ω cm, providing good evidence that the synthesis of TCO materials by CHFS can readily be scaled up, without significant deterioration in materials performance.

Acknowledgements

The EPSRC is thanked for funding the project 'Sustainable Manufacturing of Transparent Conducting Oxide (TCO) Inks and Thin Films' (reference number EP/L017709/1).

Supporting Information

Comprehensive description and diagrams of reactor configurations. Hall probe data for In_2O_3 and ITO samples.

References

(1) Edwards, P. P.; Porch, A.; Jones, M. O.; Morgan, D. V; Perks, R. M. Basic Materials Physics of Transparent Conducting Oxides. *Dalton Trans.* **2004**, No. 19, 2995–3002.

(2) Chopra, K.; Major, S.; Pandya, D. Transparent Conductors—a Status Review. *Thin Solid Films* **1983**, *102*, 1–46.

(3) Calnan, S.; Tiwari, A. N. High Mobility Transparent Conducting Oxides for Thin Film Solar Cells. *Thin*

Solid Films **2010**, *518* (7), 1839–1849.

(4) Granqvist, C. .; Azens, A.; Hjelm, A.; Kullman, L.; Niklasson, G. .; Rönnow, D.; Strømme Mattsson, M.; Veszelei, M.; Vaivars, G. Recent Advances in Electrochromics for Smart Windows Applications. *Sol. Energy* **1998**, *63* (4), 199–216.

(5) Park, J.-W.; Lee, G.-H.; Kwon, Y. Y.; Park, K.-W.; Lee, J.; Jin, Y. W.; Nah, Y.-C.; Kim, H. Enhancement in Light Extraction Efficiency of Organic Light Emitting Diodes Using Double-Layered Transparent Conducting Oxide Structure. *Org. Electron.* **2014**, *15* (10), 2178–2183.

(6) Gordon, R. Criteria for Choosing Transparent Conductors. *MRS Bull.* **2000**, No. August, 52–57.

(7) Minami, T. Transparent Conducting Oxide Semiconductors for Transparent Electrodes. *Semicond. Sci. Technol.* **2005**, *20* (4), S35–S44.

(8) Bel Hadj Tahar, R.; Ban, T.; Ohya, Y.; Takahashi, Y. Tin Doped Indium Oxide Thin Films: Electrical Properties. *J. Appl. Phys.* **1998**, *83* (5), 2631.

(9) Stadler, A. Transparent Conducting Oxides—An Up-To-Date Overview. *Materials (Basel).* **2012**, *5* (12), 661–683.

(10) Sittinger, V.; Ruske, F.; Werner, W.; Jacobs, C.; Szyszka, B.; Christie, D. J. High Power Pulsed Magnetron Sputtering of Transparent Conducting Oxides. *Thin Solid Films* **2008**, *516* (17), 5847–5859.

(11) Maruyama, T.; Fukui, K. Indium-Tin Oxide Thin Films Prepared by Chemical Vapor Deposition. *J. Appl. Phys.* **1991**, *70* (7), 3848.

(12) Kawazoe, H.; Yasukawa, M.; Hyodo, H.; Kurita, M.; Yanagi, H.; Hosono, H. P-Type Electrical Conduction in Transparent Thin Films of CuAlO2. *Nature* **1997**, *389* (6654), 939–942.

(13) Bühler, G.; Thölmann, D.; Feldmann, C. One-Pot Synthesis of Highly Conductive Indium Tin Oxide Nanocrystals. *Adv. Mater.* **2007**, *19* (17), 2224–2227.

(14) Hwang, M.; Jeong, B.; Moon, J.; Chun, S.-K.; Kim, J. Inkjet-Printing of Indium Tin Oxide (ITO) Films for Transparent Conducting Electrodes. *Mater. Sci. Eng. B* **2011**, *176* (14), 1128–1131.

(15) Al-Dahoudi, N.; Aegerter, M. A. Wet Coating Deposition of ITO Coatings on Plastic Substrates. *J. Sol-Gel Sci. Technol.* **2003**, *26* (1-3), 693–697.

(16) Street, R. A.; Wong, W. S.; Ready, S. E.; Chabinyc, M. L.; Arias, A. C.; Limb, S.; Salleo, A.; Lujan, R. Jet Printing Flexible Displays. *Mater. Today* **2006**, *9* (4), 32–37.

(17) Lee, J.-S.; Choi, S.-C. Solvent Effect on Synthesis of Indium Tin Oxide Nano-Powders by a Solvothermal Process. *J. Eur. Ceram. Soc.* **2005**, *25* (14), 3307–3314.

(18) Sasaki, T.; Endo, Y.; Nakaya, M.; Kanie, K.; Nagatomi, A.; Tanoue, K.; Nakamura, R.; Muramatsu, A. One-Step Solvothermal Synthesis of Cubic-Shaped ITO Nanoparticles Precisely Controlled in Size and Shape and Their Electrical Resistivity. *J. Mater. Chem.* **2010**, *20* (37), 8153.

(19) Ito, D.; Masuko, K.; Weintraub, B. a.; McKenzie, L. C.; Hutchison, J. E. Convenient Preparation of ITO Nanoparticles Inks for Transparent Conductive Thin Films. *J. Nanoparticle Res.* **2012**, *14* (12), 1274.

(20) DeLacy, B. G.; Lacey, S.; Zhang, D.; Valdes, E.; Hoang, K. Controlling the Morphology of Indium Tin Oxide Using PEG-Assisted Hydrothermal Synthesis. *Mater. Lett.* **2014**, *117*, 108–111.

(21) Ba, J.; Fattakhova Rohlfing, D.; Feldhoff, A.; Brezesinski, T.; Djerdj, I.; Wark, M.; Niederberger, M. Nonaqueous Synthesis of Uniform Indium Tin Oxide Nanocrystals and Their Electrical Conductivity in Dependence of the Tin Oxide Concentration. *Chem. Mater.* **2006**, *18* (12), 2848–2854.

(22) Hammarberg, E.; Prodi-Schwab, A.; Feldmann, C. Microwave-Assisted Synthesis of Indium Tin Oxide Nanocrystals in Polyol Media and Transparent, Conductive Layers Thereof. *Thin Solid Films* **2008**, *516* (21), 7437–7442.

(23) Adschiri, T.; Kanazawa, K.; Arai, K. Rapid and Continuous Hydrothermal Crystallization of Metal Oxide Particles in Supercritical Water. *J. Am. …* **1992**, *22* (196504), 1019–1022.

(24) Ma, C. Y.; Wang, X.; Tighe, C. J.; Darr, J. A. Modelling and Simulation of Counter-Current and Confined Jet Reactors for Continuous Hydrothermal Flow Synthesis of Nano-Materials. In *Advanced Control of Chemical Processes*; 2012; Vol. 8, pp 874–879.

(25) Gruar, R. I.; Tighe, C. J.; Darr, J. A. Scaling-up a Confined Jet Reactor for the Continuous Hydrothermal Manufacture of Nanomaterials. *Ind. Eng. Chem. Res.* **2013**, *52* (15), 5270–5281.

(26) Darr, J. A.; Tighe, C. J.; Gruar, R. I. Co-current Mixer, Apparatus, Reactor and Method for Precipitating Nanoparticles, U.S. Patent 20130136687, October 2, 2013.

(27) Tighe, C. J.; Cabrera, R. Q.; Gruar, R. I.; Darr, J. A. Scale Up Production of Nanoparticles: Continuous Supercritical Water Synthesis of Ce–Zn Oxides. *Ind. Eng. Chem. Res.* **2013**, *52* (16), 5522–5528.

(28) Goodall, J. B. M.; Illsley, D.; Lines, R.; Makwana, N. M.; Darr, J. A. Structure-Property-Composition Relationships in Doped Zinc Oxides: Enhanced Photocatalytic Activity with Rare Earth Dopants. *ACS Comb. Sci.* **2015**, *17* (2), 100–112.

(29) Weng, X.; Cockcroft, J. K.; Hyett, G.; Vickers, M.; Boldrin, P.; Tang, C. C.; Thompson, S. P.; Parker, J. E.; Knowles, J. C.; Rehman, I.; Parkin, I.; Evans, J. R. G.; Darr, J. A. High-Throughput Continuous Hydrothermal Synthesis of an Entire Nanoceramic Phase Diagram. *J. Comb. Chem.* **2009**, *11* (5), 829–834.

(30) Lin, T.; Kellici, S.; Gong, K.; Thompson, K.; Evans, J. R. G.; Wang, X.; Darr, J. A. Rapid Automated Materials Synthesis Instrument: Exploring the Composition and Heat-Treatment of Nanoprecursors toward Low Temperature Red Phosphors. *J. Comb. Chem.* **2010**, *12* (3), 383–392.

(31) Alexander, S. J.; Lin, T.; Brett, D. J. L.; Evans, J. R. G.; Cibin, G.; Dent, A.; Sankar, G.; Darr, J. A. A Combinatorial Nanoprecursor Route for Direct Solid State Chemistry: Discovery and Electronic Properties of New Iron-Doped Lanthanum Nickelates up to La4Ni2FeO10−δ. *Solid State Ionics* **2012**, *225*, 176–181.

(32) Elouali, S.; Bloor, L. G.; Binions, R.; Parkin, I. P.; Carmalt, C. J.; Darr, J. a. Gas Sensing with Nano-Indium Oxides (In2O3) Prepared via Continuous Hydrothermal Flow Synthesis. *Langmuir* **2012**, *28* (3), 1879–1885.

(33) Naik, A. J. T.; Gruar, R.; Tighe, C. J.; Parkin, I. P.; Darr, J. A.; Binions, R. Environmental Sensing Semiconducting Nanoceramics Made Using a Continuous Hydrothermal Synthesis Pilot Plant. *Sensors Actuators B Chem.* **2014**.

(34) Fang, Z.; Assaaoudi, H.; Guthrie, R. I. L.; Kozinski, J. A.; Butler, I. S. Continuous Synthesis of Tin and Indium Oxide Nanoparticles in Sub- and Supercritical Water. *J. Am. Ceram. Soc.* **2007**, *90* (8), 2367–2371.

(35) Lu, J.; Minami, K.; Takami, S.; Shibata, M.; Kaneko, Y.; Adschiri, T. Supercritical Hydrothermal Synthesis and in Situ Organic Modification of Indium Tin Oxide Nanoparticles Using Continuous-Flow Reaction System. *ACS Appl. Mater. Interfaces* **2012**, *4* (1), 351–354.

(36) Frank, G.; Kostlin, H. Electrical Properties and Defect Model of Tin-Doped Indium Oxide Layers. *Appl. Phys. A Solids Surfaces* **1982**, *27* (4), 197–206.

(37) Kim, N.-R.; Lee, J.-H.; Lee, Y.-Y.; Nam, D.-H.; Yeon, H.-W.; Lee, S.-Y.; Yang, T.-Y.; Lee, Y.-J.; Chu, A.; Nam, K. T.; Joo, Y.-C. Enhanced Conductivity of Solution-Processed Indium Tin Oxide Nanoparticle Films by Oxygen Partial Pressure Controlled Annealing. *J. Mater. Chem. C* **2013**, *1* (37), 5953.

(38) Fan, J. C. C.; Goodenough, J. B. X-Ray Photoemission Spectroscopy Studies of Sn-Doped Indium-Oxide Films. *J. Appl. Phys.* **1977**, *48* (8), 3524.

(39) Zhang, Y.; Zhang, J.; Zhao, L.; Sheng, C. Decomposition of Formic Acid in Supercritical Water †. *Energy & Fuels* **2010**, *24* (1), 95–99.

(40) Yu, J.; Savage, P. E. Decomposition of Formic Acid under Hydrothermal Conditions. *Ind. Eng. Chem. Res.* **1998**, *37* (1), 2–10.

(41) Wagner, W. The IAPWS Formulation 1995 for the Thermodynamic Properties of Ordinary Water Substance for General and Scientific Use. *J. Phys. Chem. Ref. Data* **1999**, *31* (2), 387.

(42) Lany, S.; Zunger, A. Dopability, Intrinsic Conductivity, and Nonstoichiometry of Transparent Conducting Oxides. *Phys. Rev. Lett.* **2007**, *98* (4), 045501.

(43) Yamaura, H.; Jinkawa, T.; Tamaki, J.; Moriya, K.; Miura, N.; Yamazoe, N. Indium Oxide-Based Gas Sensor for Selective Detection of CO. *Sensors Actuators B Chem.* **1996**, *36* (1-3), 325–332.

(44) Stranick, M. A. SnO2 by XPS. *Surf. Sci. Spectra* **1993**, *2* (1), 50.

(45) Tomonaga, H.; Morimoto, T. Indium–tin Oxide Coatings via Chemical Solution Deposition. *Thin Solid Films* **2001**, *392* (2), 243–248.

(46) Hamberg, I.; Granqvist, C. G. Evaporated Sn-Doped In2O3 Films: Basic Optical Properties and

Applications to Energy-Efficient Windows. *J. Appl. Phys.* **1986**, *60* (11), R123.

(47) Oghbaei, M.; Mirzaee, O. Microwave versus Conventional Sintering: A Review of Fundamentals, Advantages and Applications. *J. Alloys Compd.* **2010**, *494* (1-2), 175–189.

For Table of Contents Only

Highly conductive indium-tin oxide (ITO) nanomaterials have been synthesised using a laboratory scale continuous hydrothermal flow synthesis (CHFS) process and the optimised composition was successfully scaled up using a pilot plant CHFS reactor at a scale of 100 g/hour.

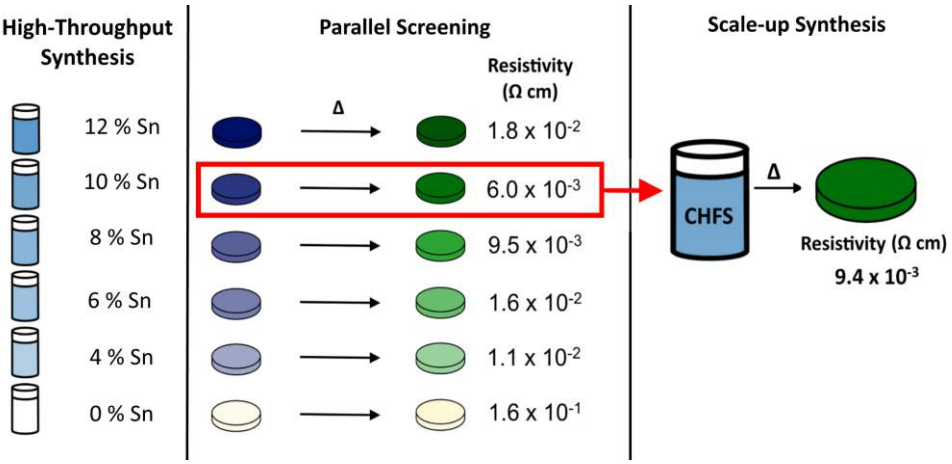

Keywords: continuous hydrothermal; transparent conducting oxides; indium tin oxide; nanoparticles; scale-up.